Nano Energy (2015) 15, 746–754

Available online at www.sciencedirect.com

ScienceDirect

journal homepage: www.elsevier.com/locate/nanoenergy

RAPID COMMUNICATION

Sulfur covalently bonded graphene with large capacity and high rate for high-performance sodium-ion batteries anodes

Xiaolei Wang[a], Ge Li[a], Fathy M. Hassan[a], Jingde Li[a], Xingye Fan[a], Rasim Batmaz[a], Xingcheng Xiao[b], Zhongwei Chen[a,*]

[a]*Department of Chemical Engineering, University of Waterloo, 200 University Avenue West, Waterloo, ON, Canada, N2L3G1*
[b]*Chemical Sciences and Materials Systems, General Motors Global Research and Development Center, 30500 Mound Road, Warren, MI 48090, United States*

Received 20 March 2015; received in revised form 28 May 2015; accepted 31 May 2015
Available online 7 June 2015

KEYWORDS
Sodium-ion battery;
Sulfur-doped graphene;
Covalent bonding;
Nanoporous;
Long stability;
High rate

Abstract
Na-ion battery is playing an important role as a low-cost alternative power source to Li-ion battery. Developing novel carbonaceous anode materials is highly demanded for high performance and environmental benignity. We report, for the first time, the graphene sheets covalently bonded with sulfur atoms as Na-ion battery anode material with a large reversible capacity of 291 mA h g^{-1} and an outstanding rate capability with 127 and 83 mA h g^{-1} at 2.0 and 5.0 A g^{-1} (charging/discharging in 3.8 and 1 min, respectively), and a long cycling stability as well. Both experiment and density functional theory calculation proves that the superior performance is mainly attributed to the unique nanoporous structure stemmed from the chemically S doping. This material holds great promise in future application of low cost, high-performance Na-ion batteries.

Introduction

There is an ever-increasing demand for the rechargeable lithium-ion batteries (LIBs) in the upcoming era of portable electronics, electric transportation and smart grids, owing to their high energy and mature fabrication technologies [1–3]. The further development and large-scale application of LIBs, however, has brought growing concern from both academia and industry in recent years regarding the increasing cost and an uneven geological distribution of lithium source [4]. By comparison, sodium (Na) is environmentally benign and is the sixth abundant element in the

*Corresponding author.
E-mail address: zhwchen@uwaterloo.ca (Z. Chen).

http://dx.doi.org/10.1016/j.nanoen.2015.05.038
2211-2855/

Earth's crust, while the sodium salts used to prepare battery materials are plentiful [5]. Furthermore, the standard electrode potential of Na/Na^+ at 2.71 V and of Li/Li^+ at 3.02 V are very close to each other, and the non-aqueous electrolytes containing sodium salts usually show similar electrochemical windows, comparable ionic conductivities and stabilities to lithium-ion counterparts [6,7]. In this context, sodium-ion based rechargeable batteries hold great promise as low-cost alternative power sources to LIBs for future energy storage technologies.

Compared to LIBs technology, the energy and power performance of SIBs cannot meet the current needs due to the limited capacity and slow kinetics of the SIBs electrodes [8]. It is well recognized that reversible and rapid sodium ions insertion and extraction is more complicated and difficult than Li^+ in host materials, due to the larger ion radius (1.02 Å of Na^+ vs. 0.76 Å of Li^+) [9]. Therefore, the key factor is to develop suitable electrode materials with sufficient interstitial space for sodium ions storage and transportation [10]. Recent research shows that many transition metal oxides [11,12], fluorophosphates [13-15], fluorosulphate [16], and ferricyanide [17-19] can serve as cathode materials with a certain capacity [20]. However, these non-carbon based inorganic materials can hardly be dominant due to the environmental benignity and cost considerations.

Although graphite, which is the dominant anode material in current LIBs technology, is not suitable for SIBs anode since no staged intercalation compounds can form [21], other carbonaceous materials still attract considerable research attention. For example, hollow carbon nanowires deliver a high reversible capacity of 251 mA h g^{-1} [22], while hollow carbon nanospheres exhibit excellent rate capability (75 mA h g^{-1} at 5.0 A g^{-1}) [23]. Many other carbon materials such as petroleum cokes [24-26], carbon black [27], template carbon [28], and hard carbon [29] have also been reported, however, the capacity and rate capability of SIBs anode are still hardly comparable to that of LIBs. It is widely accepted that the sodium insertion mechanism strongly depends on the size, the graphitization degree, the structure or textural disorder, and the porosity [30]. In this context, developing novel carbon-based anode materials with high reversible capacity and rate capability is still challenging and urgently needed.

Herein, we report for the first time the utilization of chemically sulfur-doped graphene (SG) as anode material for high-performance sodium-ion based energy storage. Recently, graphene has been attracting tremendous interest due to its unique two-dimensional, single atomic layer structure. Different from graphite with well ordered layers which is not favorable for Na^+ insertion, graphene with a few layers stack shows improved sodium storage property [31,32]. In this work, benefiting from the sulfur atoms covalently bonded to the graphene sheets, the obtained SG material exhibits a high reversible capacity of 291 mA h g^{-1}, a long stability over 200 cycles, and a superior rate capability (83 mA h g^{-1} at 5.0 A) as well, which is mainly attributed to the electronic structure changes in graphene sheets.

Results and discussion

The SG was prepared starting from graphene oxide (GO) using phenyl disulfide (PDS) as the sulfur precursor through a high-temperature flash heat treatment, where the sulfur atoms and graphene sheets covalently bond together. The morphology and microstructure of the chemically S-doped graphene were characterized by scanning electron microscope (SEM) and transmission electron microscope (TEM). Figure 1A shows the representative SEM image of the as-prepared SG material. Similar to pure graphene materials, a two-dimensional sheet-like structure with wrinkled and folded features was obtained. Figure 1B shows the representative TEM image of the as-prepared SG material. Transparent and crumpled silk veil-like structures with single or a few graphene layers can be clearly observed. In order to confirm the presence of element sulfur in SG, the elemental composition analysis from EDX pattern was applied, showing ~2.52% S exists in atomic ratio (Figure 1C). The distribution of S atoms is further verified by EDS element mapping. As shown in Figure 1D, the S atoms are uniformly dispersed in the graphene sheets, indicating the successful formation of chemically S-doped graphene. The electron energy loss spectroscopy (EELS) was also performed, confirming the existence of element C and S in SG. Based on the EELS analysis, the S content in the SG is 2.29% in atomic ratio (Figure S1).

In order to investigate how sulfur atoms are covalently bonded to graphene sheets, X-ray photoelectron spectroscopy (XPS) measurements were carried out (Figure S2). Figure 2A shows the XPS core-level spectrum of S 2p, where two major peaks locating at 163.74 and 164.92 eV can be observed, indicating a significant amount of S (3.33%). The doublet possesses an area ratio of 2:1 with a splitting of 1.18 eV, which well matches the standard value [33]. The lower energy shift (164.00 eV for standard S $2p_{3/2}$) of S $2p_{3/2}$ and $2p_{1/2}$ doublet is associated with lower valence states, suggesting the covalent bonding of S atoms to carbon atoms in a heterocyclic configuration. Four minor peaks can also be found at higher energy, which can be attributed to a small amount of carbon bonded SO_x species [34]. Obviously, in the corresponding structural scheme of SG material shown in Figure 2B, the C-S-C species exist in the thiophene form residing on the edge plane and defect sites of SG, which is the dominant S dopants in SG materials (~79%, Table S1). The existence of minor peaks of C 1s at higher energy from the core-level spectrum also implies the successful doping of S atoms with C (Figure S3). Figure 2C shows the representative X-ray diffraction pattern of SG material, with the characteristic (002) peak of graphite observed at 25.6°. The interlayer distance of SGs was calculated to be 0.348 nm, which was larger than that of graphite crystal structure with 0.335 nm. No obvious peaks from pure sulfur can be observed, further confirming the absence of element S. The porous structure of SG is characterized by the nitrogen adsorption-desorption isotherms. As shown in Figure 2D, the SG material exhibits a type IV isotherm with a Brunauer-Emmett-Teller (BET) surface area of 280 m^2 g^{-1}. Besides, the SG material possesses both micropores below 2 nm and mesopores generated from SG crumpling and piling (Figure 2D, inset).

The Na^+ insertion/extraction behavior in SG was first investigated by cyclic voltammetry using 2032-tpye coin-cells with sodium foil as the counter electrode. The mass loading of active materials in each electrode was controlled to be 1.2 mg cm^{-2}. Figure 3A shows the cyclic

voltammograms (CV) of the SG electrode for the first 10 cycles at a scan rate of 0.1 mV s^{-1} between 3.0 to 0.001 V (vs. Na/Na^+). During the first cathodic scan, an irreversible reductive peak can be found locating at 0.43 V, corresponding to the decomposition of the electrolyte and the formation of solid electrolyte interface (SEI) on the surface of the SG. A sharp peak is observed at lower voltage, corresponding to the sodium insertion, which is similar to that of the lithium insertion process in carbonaceous materials [35,36]. During the anodic scan, no obvious sharp peak can be found, indicating the sodium extraction process occurs over a broad potential range from 0 to ~1.30 V, which is consistent with previous reports [23]. In the following cycles, the CV curves show a pair of redox peaks at 1.00 V for cathodic scan and 1.77 V for anodic scan, respectively, with good repeatability. This interesting phenomenon is reported for the first time, and can be attributed to the reversible interaction of Na^+ with S dopants. Besides, a small anodic peak at 0.09 V is observed, originating from the sodium extraction from nanopores [23]. Figure 3B displays the galvanostatic charge–discharge curves of SG electrode at a current density of 50 mA g^{-1} between 3.0 to 0.001 V (vs. Na/Na^+). The SG electrode delivers an initial discharge capacity of 727 mA h g^{-1}, and a recovered charge capacity of only 417 mA h g^{-1}. The large irreversible capacity loss is mainly from the formation of SEI layer, which is consistent with the CV observation. Plateaus at around 1.0 V from discharge curves and at around 1.7 V from charge curves for the following cycles can be clearly found, indicating the redox reaction between Na^+ and S atoms observed in CV testing. Interestingly, this phenomenon can be found in SG materials with different S ratios (by adjusting the amount of PDS precursor), while no obvious plateaus can be observed in pure graphene materials (Figure S4). This is a direct evidence of reversible interaction between Na^+ and S atoms.

The capacity gradually decreases and stabilizes (291 mA h g^{-1} for the 10th cycle), forming the intercalation compound equivalent to $NaC_{7.7}$, which is very close to the lithium counterpart (LiC_6). The gradual capacity loss for the

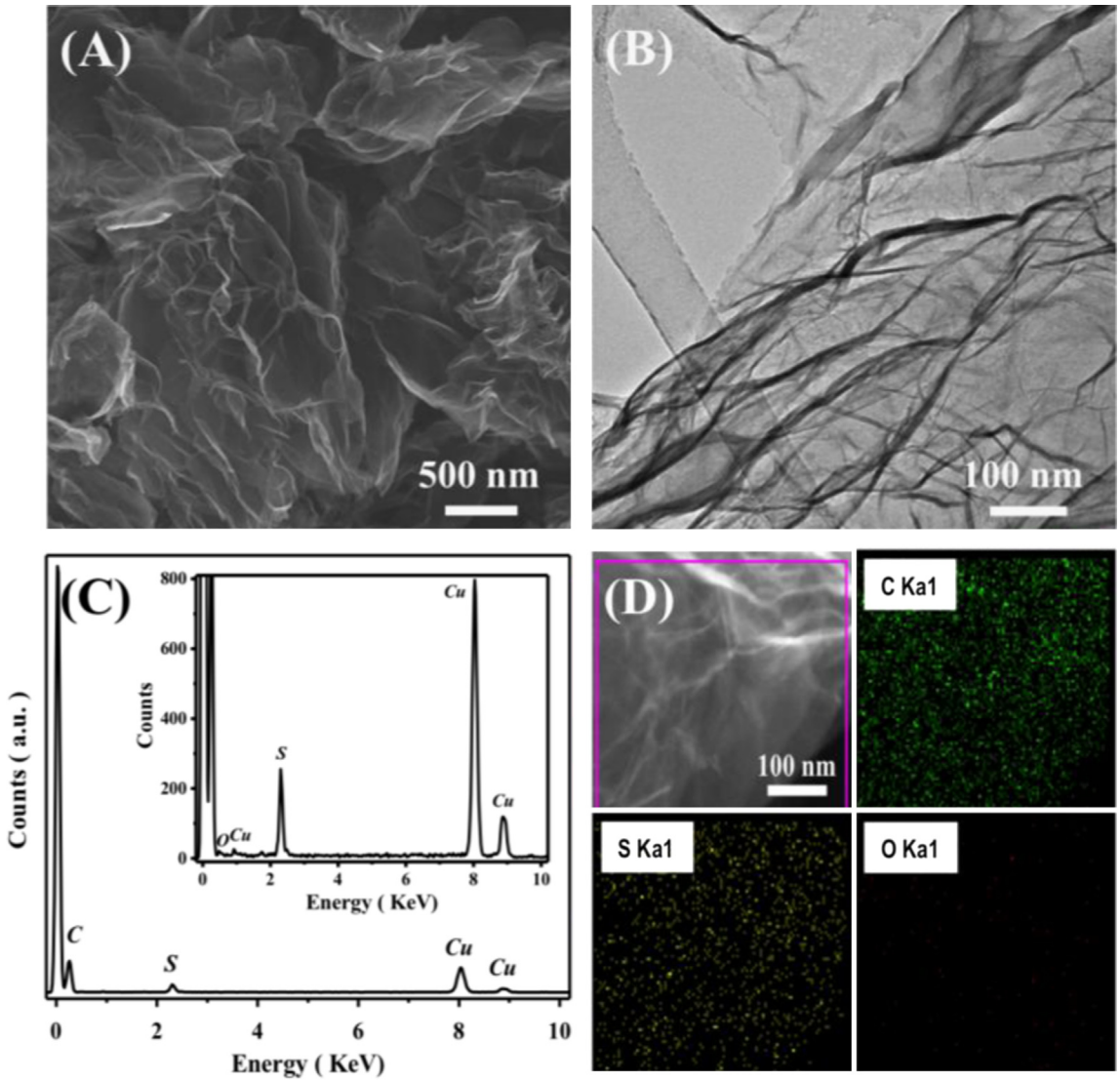

Figure 1 (A) SEM and (B) TEM images of as-prepared SG sheets; (C) EDX pattern of SG materials; and (D) STEM image of a selected area of SG and the corresponding elemental mapping showing the distribution of C–K, S–K, and O–K.

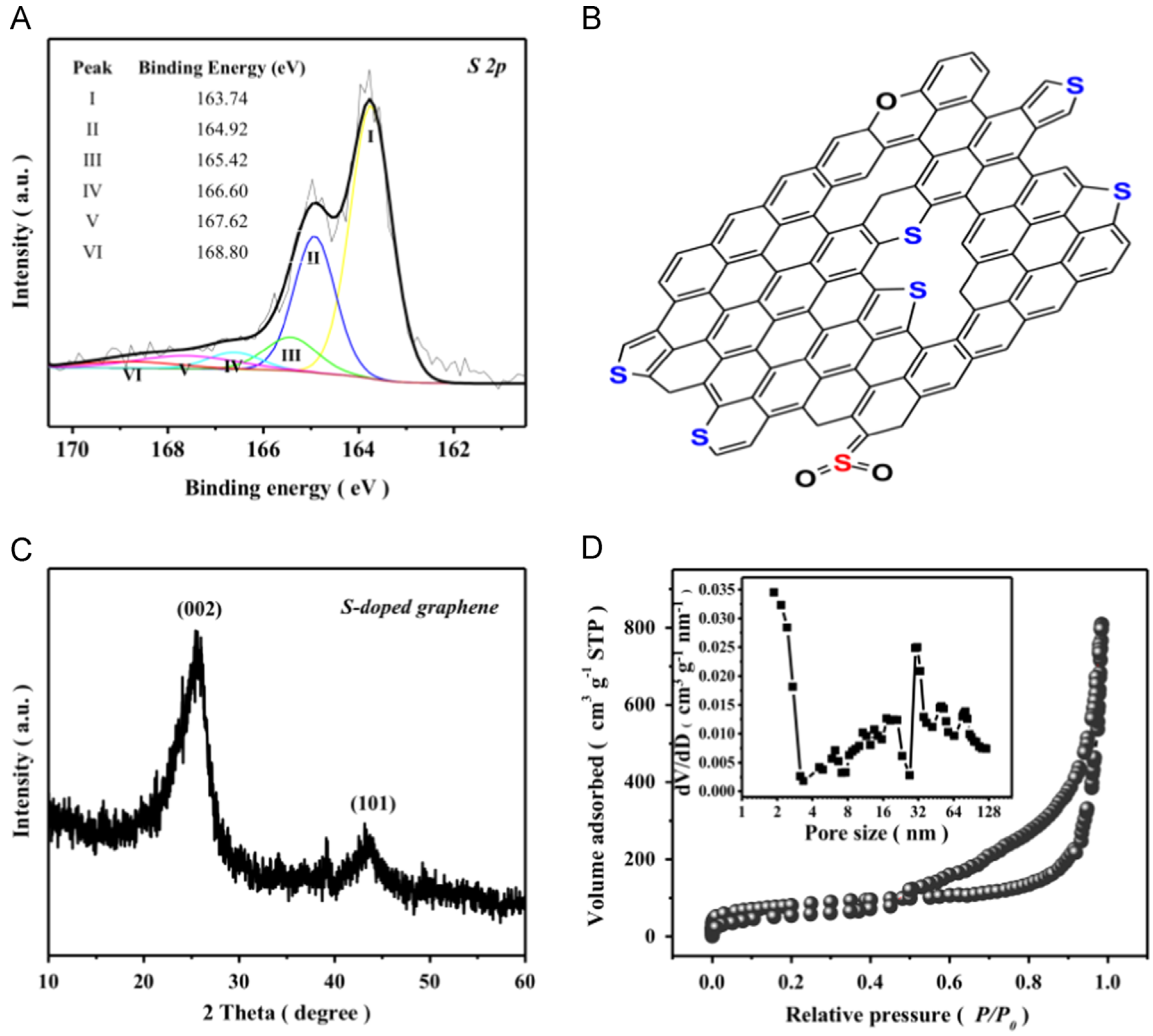

Figure 2 (A) XPS spectra of S 2p in SG material; (B) schematic model of SG material showing different S-containing functional groups; (C) XRD pattern of the SG material; and (D) nitrogen adsorption-desorption isotherm and pore-size distribution curve (inset) of the SG material.

first few cycles can be ascribed to the SEI formation on newly exposed surface from the interfaces of overlapped SG layers. Figure 3C presents the cyclability of the SG electrode at a current density of 50 mA g^{-1} for 15 cycles and at a 1.0 A g^{-1} for 200 cycles. After 200 cycles, the SG electrode still possesses a capacity of 150 mA h g^{-1}, a high capacity retention of 80% can be obtained along with the high Coulombic efficiency. The gradual capacity decay is commonly found in carbon-based materials for SIBs as well as graphene-based materials for LIBs anode, suggesting that the interaction of Na^+ with S atoms is highly reversible. This is further confirmed by XPS analysis of S element (Figure S5), where the S $2p_{3/2}$ peak from core-level spectrum is observed locating at 161.96 eV. Compared with 163.74 eV for pristine SG, the significant peak shift to even lower energy suggests the lower oxidation state of S atoms, which is mainly ascribed to the strong interaction between Na^+ and S atoms. Such a cycling stability is mainly due to the covalently bonded S atoms to the graphene sheets. Although an increased I_D/I_G value can be obtained from the Raman spectra (Figure S6) after cycling (from 0.836 to 1.012), reflecting a increased defects of SG materials, the SG sheets still remain the morphology (Figure S7). Moreover, the TEM image of the SG material after cycling further confirms the reversible process. As shown in Figure 3D, the S atoms still exist, and are homogeneously distributed, while the fluorine element is mainly from the PVdF binder.

The excellent cycling stability can be further revealed at high current densities. As shown in Figure 3E, the SG electrodes were activated for five cycles at a current density of 100 mA g^{-1}, and then cycled for 100 cycles at 2.0 and 5.0 A g^{-1}, respectively. After 100 cycles at 2.0 A g^{-1}, the SG electrode still possesses a discharge capacity of 133 mA h g^{-1}, ~83% of the initial capacity can be obtained; while after 100 cycles at 5.0 A g^{-1}, a 74% capacity retention can be achieved. Figure 3F exhibits the Nyquist plots of SG electrode at different cycles at the current density of 2.0 A g^{-1}. Each plot consists of a semicircle at high- and middle-frequency and a linear Warburg tail at low frequency. The intercept of the plot with the real axis at high frequency corresponds to the bulk resistance of the electrolyte, while the semi-circle reflects the resistance of ions

migration through the SEI layer. The Warburg tail usually represents the ion-diffusion resistance in the electrode materials and structure [37]. The resistance of the SG electrode increases in the first 50 cycles and then stabilizes. Similar phenomena were also reported on carbon-based electrodes for LIBs and SIBs. Such an electrochemical impedance spectra (EIS) characteristic further confirms the SG electrode is highly robust.

In addition to the high reversible capacity and long stability, SG electrodes also exhibit excellent rate capabil-

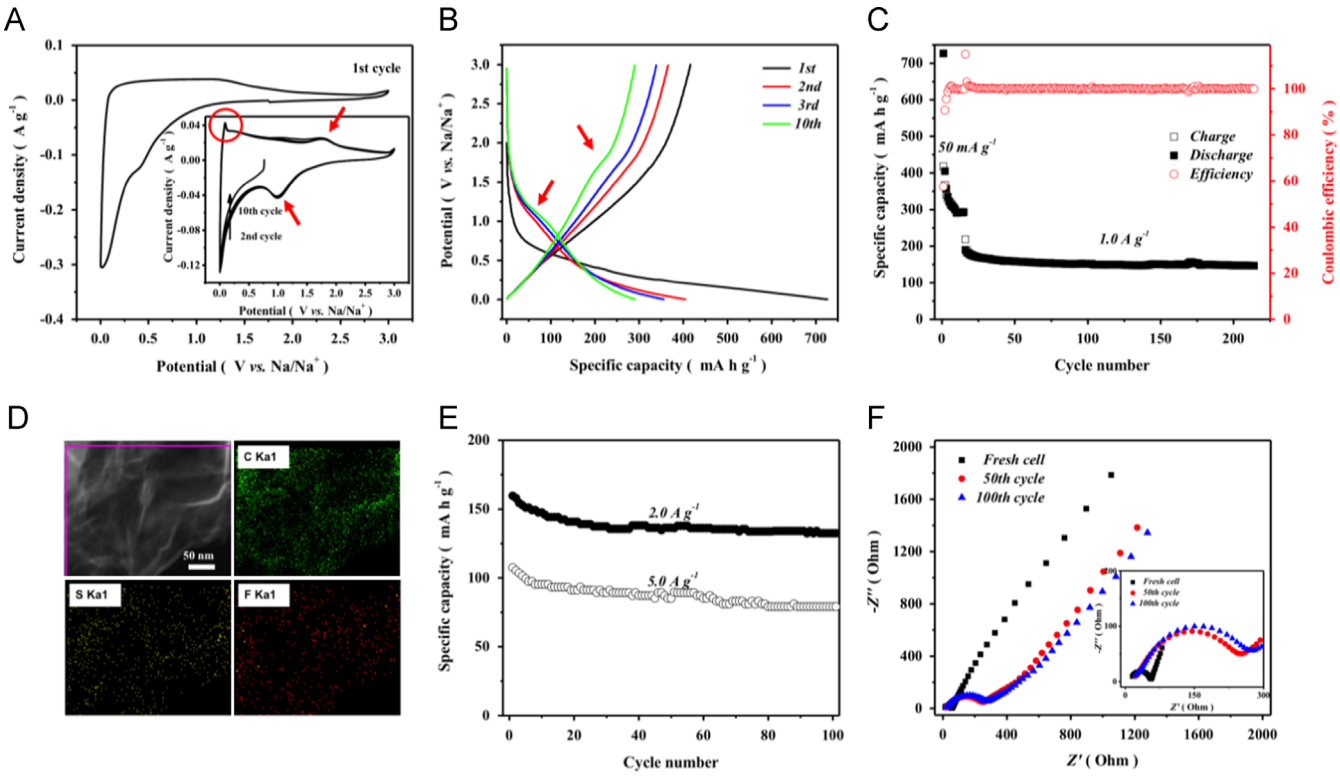

Figure 3 (A) CV curves of SG electrode at a scan rate of 0.1 mV s^{-1} between 3.000 and 0.001 V for the first 10 cycles; (B) galvanostatic charge–discharge curves of the SG electrode at a current density of 50 mA g^{-1} between 3.000 and 0.001 V for the first, second, third, and 10th cycle; (C) corresponding cycling performance of the SG electrode at 50 mA g^{-1} for 15 cycles and at 1.0 A g^{-1} for 200 cycles; (D) high-angle annular dark field scanning transmission electron micrograph (HAADF-STEM) of the SG electrode material after cycling, and the EDS elemental mapping of C, S and F for the area selected; (E) cycling performance of SG electrodes at 2.0 and 5.0 A g^{-1} for 100 cycles; and (F) Nyquist plots of the SG electrode at fresh state and after 50 and 100 cycles of galvanostatic charge–discharge at 2.0 A g^{-1} over the frequency range from 100 kHz to 0.01 Hz (Inset shows enlarged spectra at high-frequency range).

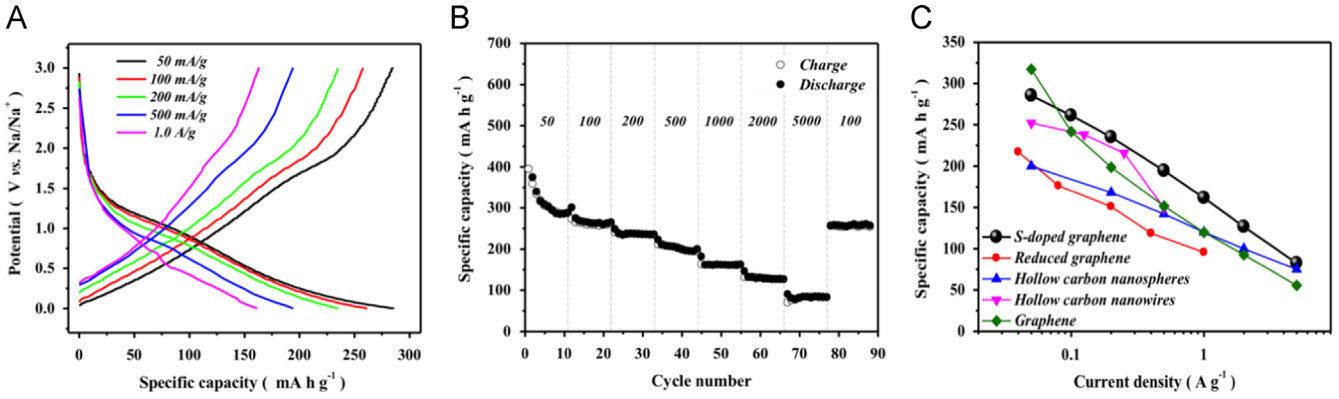

Figure 4 (A) Galvanostatic charge–discharge profiles of SG electrode at various current densities from 50 mA g^{-1} to 1.0 A g^{-1} between 3.000 and 0.001 V; (B) corresponding rate capability of the SG electrode; and (C) comparison of the rate capability of various carbon-based high-rate SIBs anodes reported recently, including reduced graphene sheets, hollow carbon nanospheres, hollow carbon nanowires, and graphene synthesized at the same condition as SG.

ity. The fast Na^+ charge-storage process was characterized by charging and discharging the SG electrodes at various current densities. As shown in Figure 4A, a reversible and stable specific discharge capacity of 262 mA h g^{-1} and 161 mA h g^{-1} can be achieved at a current density of 100 mA g^{-1} and 1.0 A g^{-1}, respectively. The corresponding capacity dependence on cycling numbers is shown in Figure 4B. Remarkably, even at a high current density of 5.0 A g^{-1}, the SG electrode can still deliver a reversible capacity of 83 mA h g^{-1} (discharging time of 59 s), corresponding to a ~30% capacity retention. Figure 4C further compares the rate performance of SG with a series of carbonaceous materials for SIBs anode, including reduced graphene [31], hollow carbon nanospheres [23], and hollow carbon nanowires [22], and pure graphene synthesized at the same condition as SG (Figure S8). Clearly, the S-doped graphene material outperforms most of the others. Such a superior rate performance is mainly attributed to the unique microstructure of the SG nanosheets [38]. On one hand, the SG materials possess an interlayer spacing of 0.348 nm determined by XRD characterization which is larger than 0.335 nm of graphite, and this difference could be more pronounced after Na^+ intercalation. The increased interlayer spacing can significantly improve the Na^+ insertion and diffusion during discharging process, which has been reported previously [22]. On the other hand, nanopores at the defect areas created from the covalent S doping offer z-axial Na^+ diffusion pathway, enabling fast accessibility of both the graphene surface and S-containing active sites, which further improves the electrode kinetics.

To further analyze how the Na^+ interacts with S atoms and passes through nanopores at the defect areas, three different SG models were designed with different vacancy sites. Figure 5A shows one of the most stable adsorption configurations of SG model, where Na^+ is residing in the nanopore created from the S doping. The corresponding binding energy is calculated to be −2.02 eV, and a little less based on different models also with most stable adsorption configurations (Figure S9 A and D). The observed moderate bonding energy indicates that Na^+ can interact with S atoms reversibly during the intercalation process. Figure 5B shows the model where Na^+ diffuses in the direction perpendicular to the SG sheet with nanopore. Intuitively, it should be difficult for Li^+ ions to diffuse from one side of pristine graphene to the other side [39], and even harder for Na^+ with bigger radius. However, as shown in Figure 5C, the diffusion barrier for Na^+ passing through the nanopore is calculated to be 1.77 eV, which means that the Na^+ can easily pass from one side to the other side of the SG plane. By comparison, SG with smaller nanopores shows higher diffusion barrier (Figure S9 B and E, C and F). Therefore, by tailoring the microstructure of the SG materials, even higher Na^+ storage capacity and rate performance could be achieved in the future.

Conclusions

We have successfully synthesized chemically S-doped graphene and demonstrated its superior electrochemical performance as SIBs anode materials. Both the experimental results and modeling analysis prove that the S dopants cannot only boost the Na^+ storage capacity but also improve the rate capability by facilitating Na^+ diffusion in the material. The performance can be further improved by tailoring the structure of the material in the future; therefore, sulfur-doped graphene materials hold great promise in the application of sodium-ion batteries.

Experimental section

Synthesis of sulfur-doped graphene (SG) sheets

The synthesis of SG has been reported in the literature [34]. Briefly, 100 mg of graphene oxide prepared by a modified Hummer method was mixed with 100 mg of phenyl disulfide (PDS) by dispersing in ethanol, drying, and grinding. The mixture was placed into a tube furnace and kept outside the heating zone until the furnace temperature reached 1000 °C. The mixture was then pushed into the heating zone and kept for 30 min under argon protection, before it was removed from the heating zone and cooled to room temperature. SG materials with different S ratios were synthesized using different amounts of PDS under the same condition (Figure S10).

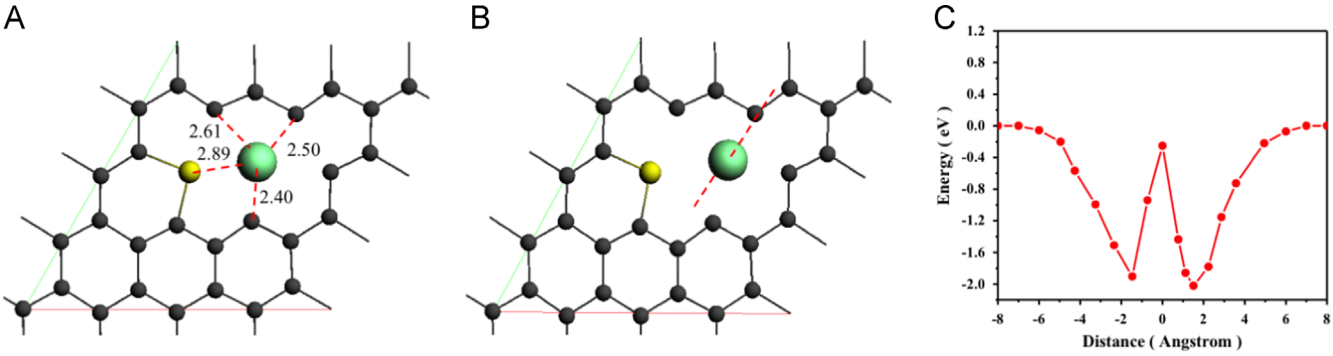

Figure 5 (A) One of the most stable adsorption configuration of SG; (B) schematic representations and (C) potential-energy curves of Na^+ diffusion near the nanopore in the direction perpendicular to the SG sheet. The green, yellow, and black balls represent sodium ion, sulfur dopant, and carbon atoms, respectively.

Material characterization

X-ray diffraction (XRD) experiments were carried out on a XRG 3000 X-ray diffractometer. Scanning electron microscopic (SEM) experiments were conducted on a LEO FESEM 1530; transmission electron microscopic (TEM) experiments and electron energy loss spectroscopy (EELS) were carried out on a JEOL 2010 F TEM/STEM field emission microscope equipped with a large solid angle for high X-ray throughput, scanning, scanning-transmission and a Gatan imaging filter (GIF) for energy filtered imaging from the Canadian Center for Electron Microscopy (CCEM) located at McMaster University. X-ray photoelectron spectroscopy (XPS) (K-Alpha XPS spectrometer, Thermal Scientific) was used to analyze chemical elements and chemical configuration.

Electrode fabrication

A conventional slurry-coating process was applied to fabricate the electrodes. The SG, SuperP, and polyvinylidene fluoride (PVdF) were mixed in a mass ratio of 8:1:1 and homogenized in N-Methyl-2-pyrrolidone to form slurries. The homogenous slurries were coated on Cu foil substrates and dried at 100 °C for 12 h under vacuum. The total mass loading on each electrode was controlled to be $\sim$1.5 mg cm^{-2}.

Electrochemical measurements

2032-type coin cells were assembled in an argon-filled glovebox, using a glass fiber separator (Whatman GF/C), sodium foils as the counter electrodes, 1 M $NaPF_6$ in a 1:1 (v/v) mixture of ethylene carbonate and dimethyl carbonate as the electrolyte. Cyclic voltammetric (CV) measurements were carried out on a VSP300 potentiostat/galvanostat (Bio-Logic LLC, Knoxville, TN) using cutoff voltages of 0.001 and 3.000 V versus Na/Na^+ at a scan rate of 0.200 mV s^{-1}. The galvanostatic charge/discharge measurements were performed on NEWARE BTS-CT3008 (Neware Technology, Ltd., Shenzhen, China) at different current densities. Electrochemical impedance spectroscopy measurement was conducted on a Princeton Applied Research VersaSTAT MC potentiostat. The Nyquist plots were recorded potentiostatically by applying an AC voltage of 10 mV amplitude in the frequency range of 0.01–100 k Hz. All electrochemical measurements were carried out at room temperature.

Computational

The DFT calculations were carried out using the program BAND [40], where the electron wave functions were developed on a basis set of numerical atomic orbitals (NAOs) and of Slater type orbitals (STOs). The triple polarization (TZP) basis of Slater-type orbitals was used. The calculations were performed by using PBE − D3 [41] generalized gradient approximation (GGA) for the exchange and correlation energy terms, which explicitly takes into account the dispersion correction. This is a widely used functional for catalysis applications and produces reliable energetics on graphene systems [42,43]. A 4×4 supercell of graphene was selected for the calculations. In all the calculations, all the atoms in the model were allowed to relax. In order to describe the interactions between the Na and SG, the bonding energies (E_{bind}) of adsorbates Na were defined by the following equation:

$$E_{bind} = E_{Na-SG} - E_{SG} - E_{Na}$$

where E_{Na-SG}, E_{SG}, and E_X represent the energies of the Na-bound to the SG structure, the SG, and the Na atom, respectively.

Acknowledgment

This work was supported by the Natural Sciences and Engineering Research Council of Canada (NSERC), University of Waterloo, and the Waterloo Institute for Nanotechnology. The authors acknowledge Dr. Carmen Andrei and Canadian Centre for Electron Microscopy for TEM characterization. The authors also acknowledge Dr. Luis Ricardez-Sandoval for computational support.

Appendix A. Supporting information

Supplementary data associated with this article can be found in the online version at http://dx.doi.org/10.1016/j.nanoen.2015.05.038.

References

[1] A.S. Arico, P. Bruce, B. Scrosati, J.-M. Tarascon, W. van Schalkwijk, Nat. Mater. 4 (2005) 366–377.
[2] A. Manthiram, J. Phys. Chem. Lett. 2 (2011) 176–184.
[3] M.S. Whittingham, MRS Bull. 33 (2008) 411–419.
[4] J.-M. Tarascon, Nat. Chem. 2 (2010) 510-510.
[5] C.J. Asher, in: J.J. Mortvedt (Ed.), Beneficial elements, functional nutrients, and possible new essential elements, Micronutrients in Agriculture, Soil Science Society of America, 1991, pp. 703–723.
[6] M.D. Slater, D. Kim, E. Lee, C.S. Johnson, Adv. Funct. Mater. 23 (2013) 947–958.
[7] D.A. Stevens, J.R. Dahn, J. Electrochem. Soc. 147 (2000) 1271–1273.
[8] S.-W. Kim, D.-H. Seo, X. Ma, G. Ceder, K. Kang, Adv. Energy Mater. 2 (2012) 710–721.
[9] K.-T. Kim, G. Ali, K.Y. Chung, C.S. Yoon, H. Yashiro, Y.-K. Sun, J. Lu, K. Amine, S.-T. Myung, Nano Lett. 14 (2014) 416–422.
[10] H.-g. Wang, Z. Wu, F.-l. Meng, D.-l. Ma, X.-l. Huang, L.-m. Wang, X.-b. Zhang, ChemSusChem 6 (2013) 56–60.
[11] Y. Sun, L. Zhao, H. Pan, X. Lu, L. Gu, Y.-S. Hu, H. Li, M. Armand, Y. Ikuhara, L. Chen, X. Huang, Nat. Commun. 4 (2013) 1870.
[12] N. Yabuuchi, M. Kajiyama, J. Iwatate, H. Nishikawa, S. Hitomi, R. Okuyama, R. Usui, Y. Yamada, S. Komaba, Nat. Mater. 11 (2012) 512–517.
[13] S.-M. Oh, S.-T. Myung, J. Hassoun, B. Scrosati, Y.-K. Sun, Electrochem. Commun. 22 (2012) 149–152.
[14] K. Chihara, A. Kitajou, I.D. Gocheva, S. Okada, J.-i. Yamaki, J. Power Sources 227 (2013) 80–85.
[15] B.L. Ellis, W.R.M. Makahnouk, Y. Makimura, K. Toghill, L. F. Nazar, Nat. Mater. 6 (2007) 749–753.
[16] N. Recham, G. Rousse, M.T. Sougrati, J.-N. Chotard, C. Frayret, S. Mariyappan, B.C. Melot, J.-C. Jumas, J.-M. Tarascon, Chem. Mater. 24 (2012) 4363–4370.
[17] C.D. Wessells, S.V. Peddada, R.A. Huggins, Y. Cui, Nano Lett. 11 (2011) 5421–5425.

[18] C.D. Wessells, R.A. Huggins, Y. Cui, Nat. Commun. 2 (2011) 550.
[19] L. Wang, Y. Lu, J. Liu, M. Xu, J. Cheng, D. Zhang, J. B. Goodenough, Angew. Chem. Int. Ed. 52 (2013) 1964–1967.
[20] V. Palomares, M. Casas-Cabanas, E. Castillo-Martinez, M. H. Han, T. Rojo, Energy Environ. Sci. 6 (2013) 2312–2337.
[21] P. Senguttuvan, G. Rousse, M.E. Arroyo y de Dompablo, H. Vezin, J.M. Tarascon, M.R. Palacín, J. Am. Chem. Soc. 135 (2013) 3897–3903.
[22] Y. Cao, L. Xiao, M.L. Sushko, W. Wang, B. Schwenzer, J. Xiao, Z. Nie, L.V. Saraf, Z. Yang, J. Liu, Nano Lett. 12 (2012) 3783–3787.
[23] K. Tang, L. Fu, R.J. White, L. Yu, M.-M. Titirici, M. Antonietti, J. Maier, Adv. Energy Mater. 2 (2012) 873–877.
[24] M.M. Doeff, Y. Ma, S.J. Visco, L.C. De Jonghe, J. Electrochem. Soc. 140 (1993) L169–L170.
[25] R. Alcántara, J.M. Jiménez Mateos, J.L. Tirado, J. Electrochem. Soc. 149 (2002) A201–A205.
[26] E. Zhecheva, R. Stoyanova, J.M. Jiménez-Mateos, R. Alcántara, P. Lavela, J.L. Tirado, Carbon 40 (2002) 2301–2306.
[27] R. Alcántara, J.M. Jiménez-Mateos, P. Lavela, J.L. Tirado, Electrochem. Commun. 3 (2001) 639–642.
[28] S. Wenzel, T. Hara, J. Janek, P. Adelhelm, Energy Environ. Sci. 4 (2011) 3342–3345.
[29] S. Komaba, W. Murata, T. Ishikawa, N. Yabuuchi, T. Ozeki, T. Nakayama, A. Ogata, K. Gotoh, K. Fujiwara, Adv. Funct. Mater. 21 (2011) 3859–3867.
[30] P. Thomas, D. Billaud, Electrochim. Acta 46 (2000) 39–47.
[31] Y.-X. Wang, S.-L. Chou, H.-K. Liu, S.-X. Dou, Carbon 57 (2013) 202–208.
[32] R. Raccichini, A. Varzi, S. Passerini, B. Scrosati, Nat. Mater. 14 (2015) 271–279.
[33] D.G. Castner, K. Hinds, D.W. Grainger, Langmuir 12 (1996) 5083–5086.
[34] D. Higgins, M.A. Hoque, M.H. Seo, R. Wang, F. Hassan, J.-Y. Choi, M. Pritzker, A. Yu, J. Zhang, Z. Chen, Adv. Funct. Mater. 24 (2014) 4325–4336.
[35] D.A. Stevens, J.R. Dahn, J. Electrochem. Soc. 148 (2001) A803–A811.
[36] J.R. Dahn, T. Zheng, Y. Liu, J.S. Xue, Science 270 (1995) 590–593.
[37] M.D. Levi, D. Aurbach, J. Phys. Chem. B 101 (1997) 4630–4640.
[38] P.A. Denis, R. Faccio, A.W. Mombru, ChemPhysChem 10 (2009) 715–722.
[39] X. Fan, W.T. Zheng, J.-L. Kuo, ACS Appl. Mater. Interfaces 4 (2012) 2432–2438.
[40] G. Wiesenekker, E.J. Baerends, J. Phys: Condens. Matter 3 (1991) 6721.
[41] S. Grimme, J. Antony, S. Ehrlich, H. Krieg, J. Chem. Phys. 132 (2010) 154104.
[42] Y. Li, Z. Chen, J. Phys. Chem. Lett. 4 (2013) 269–275.
[43] A.A. Arabi, A.D. Becke, J. Phys. Chem. Lett. 137 (2012) 014104.

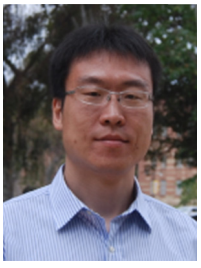

Dr. Xiaolei Wang received his master's degree from Tianjin University in 2007, and then obtained his Ph.D. in Chemical Engineering from University of California, Los Angeles in 2013. Currently, he is a postdoctoral researcher in University of Waterloo, Canada. His research interest mainly focuses on design and development of advanced materials for energy storage applications.

Dr. Ge Li obtained her Ph.D. in 2012 from East China Normal University, P.R. China. She was a visiting student in University of California, Los Angles from 2010 to 2012. She joined University of Waterloo as a postdoctoral researcher in 2014. Currently, she is working on development of composite materials for supercapacitors and lithium-sulfur batteries.

Dr. Fathy M. Hassan obtained his Ph.D. in Physical Chemistry from Cairo University in 2004. He held the Japan Society for Promotion of Science Award for foreign scientists at the National Institute of Advanced Industrial Science and Technology. He obtained his second Ph.D. in Chemical Engineering from University of Waterloo in 2014. Currently, he is a postdoctoral fellow at University of Waterloo with research interest spanning the area of nano-architecture materials for advanced electrochemical energy storage and conversion devices.

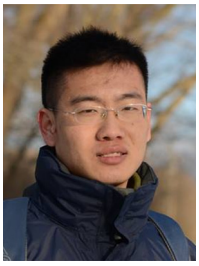

Dr. Jingde Li received his Ph.D. in Chemical Engineering, University of Waterloo in 2014. He continues his research as a postdoctoral fellow on DFT calculation of energy materials.

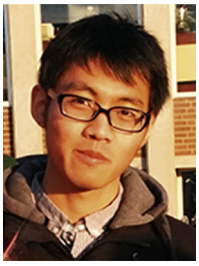

Mr. Xingye Fan is currently a master student from Department of Chemical Engineering in University of Waterloo. He mainly focuses on design and synthesis of carbon-based materials for supercapacitors and lithium-ion batteries.

Mr. Rasim Batmaz is now a Ph.D. candidate in Chemical Engineering, University of Waterloo. Currently, he is working on synthesis and electrochemical characterization of carbon-based materials.

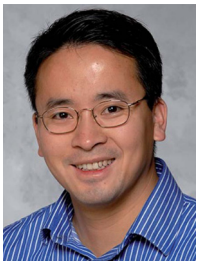

Dr. Xingcheng Xiao obtained his Ph.D. degree from the Chinese Academy of Sciences. He worked as a research associate at the Argonne National Laboratory and Brown University before joining the GM Global R&D Center in 2006. He has published over 100 peer-reviewed journal papers, and has 25 awarded patents, and 20 pending patent applications in different fields. He is the recipient of Alexander von Humboldt Fellowship, R&D 100 Award, and SME Innovations That Could Change the Way We Manufacture.

Prof. Zhongwei Chen is an Associate Professor in the Department of Chemical Engineering at University of Waterloo. His current research interests are in the development of advanced electrode materials for metal–air batteries, lithium-ion batteries and fuel cells. He received his Ph.D. in Chemical and Environmental Engineering from the University of California-Riverside. Prior to joining the faculty at Waterloo in 2008, he was focusing on the advanced catalysts research in the Los Alamos National Laboratory (LANL) at New Mexico, USA. He has published 1 book, 4 book chapters and more than 100 peer reviewed journal articles. These publications have earned him to date over 4000 citations with H-index 32. He is also listed as inventor on 3 US patents and 8 provisional US patents, with two licensed to startup companies in USA.